引用格式：LU Yi，YAN Jian-chang，LI Xiao-hang，*et al*. Carrier Manipulation and Performance Enhancement of N-polar AlGaN-based LED with Grading Quantum Barriers[J]. *Acta Photonica Sinica*，2019，**48**(7)：0723001
陆义，闫建昌，李晓航，等.具有渐变量子垒的氮极性 AlGaN 基 LED 实现载流子调控和性能增强[J].光子学报，2019，**48**(7)：0723001

具有渐变量子垒的氮极性 AlGaN 基 LED 实现载流子调控和性能增强

陆义[1,2,3,4]，闫建昌[1,2,3]，李晓航[4]，郭亚楠[1,2,3]，吴卓辉[1,2,3]，
张亮[1,2,3]，谷文[1,2,3]，王军喜[1,2,3]，李晋闽[1,2,3]

（1 中国科学院半导体研究所 半导体照明研发中心，北京 100083）
（2 中国科学院大学 材料科学与光电技术学院，北京 100049）
（3 北京市第三代半导体材料及应用工程技术研究中心，北京 100083）
（4 阿卜杜拉国王科技大学 先进半导体实验室，图沃 23955-6900，沙特阿拉伯）

摘　要：为了获得高效率的 AlGaN 基深紫外发光二极管，提出了具有渐变量子垒的氮极性结构来调控载流子的传输.通过氮极性结构在 p 型电子阻挡层中形成的反向极化诱导势垒，改善空穴注入和电子泄漏问题.另外研究了不同的渐变方向和渐变程度对器件性能的影响.模拟结果显示，在 12 nm 的 AlGaN 量子垒上沿着(000-1)方向从 Al 组分 0.65 线性渐变到 0.6，可以有效平衡量子垒的势垒高度和斜率，从而极大的增强空穴注入，光输出功率相较于传统结构提高了 53.6%.该设计为电子泄漏和空穴注入问题提供了直接而有效的解决方案，在实现更高效率的深紫外发光二极管方面显示出广阔的前景.

关键词：深紫外 LED；AlGaN；氮极性；渐变量子垒；载流子调控
中图分类号：TN312+.8　　**文献标识码**：A　　**doi**：10.3788/gzxb20194807.0723001

Carrier Manipulation and Performance Enhancement of N-polar AlGaN-based LED with Grading Quantum Barriers

LU Yi[1,2,3,4], YAN Jian-chang[1,2,3], LI Xiao-hang[4], GUO Ya-nan[1,2,3], WU Zhuo-hui[1,2,3], ZHANG Liang[1,2,3], GU Wen[1,2,3], WANG Jun-xi[1,2,3], LI Jin-min[1,2,3]

(1 *Research and Development Center for Solid-State Lighting, Institute of Semiconductors, Chinese Academy of Sciences, Beijing* 100083, *China*)
(2 *Center of Materials Science and Optoelectronics Engineering, University of Chinese Academy of Sciences, Beijing* 100049, *China*)
(3 *Beijing Engineering Research Center for the 3rd Generation Semiconductor Materials and Application, Beijing* 100083, *China*)
(4 *Advanced Semiconductor Laboratory, King Abdullah University of Science and Technology, Thuwal* 23955-6900, *Saudi Arabia*)

Foundation item: The National Key Research and Development Program of China (Nos. 2016YFB0400803, 2016YFB0400802, 2017YFB0404202), the National Natural Sciences Foundation of China (Nos. 61527814, 61674147, U1505253), Beijing Nova Program (No. Z181100006218007), Youth Innovation Promotion Association CAS (No. 2017157), King Abdullah University of Science and Technology (KAUST) Baseline (No. BAS/1/1664-01-01), KAUST Competitive Research Grant (Nos. URF/1/3437-01-01, URF/1/3771-01-01), KAUST GCC (No. REP/1/3189-01-01), National Natural Science Foundation of China (No. 61774065)
First author: LU Yi (1995－), male, M.S. degree candidate, mainly focuses on the AlGaN-based LED. Email: luyi@semi.ac.cn
Supervisor (Contact author): YAN Jian-chang (1982－), male, professor, Ph.D. degree, mainly focuses on solid state lighting. Email: yanjc@semi.ac.cn
Received: Apr.2, 2019; **Accepted**: May 5, 2019

Abstract: To achieve efficient AlGaN-based Deep Ultraviolet Light-Emitting Diode (DUV LED), the N-polar LED structure with grading quantum barriers is proposed to manipulate the carrier transport. By adopting the N-polar structure, the hole injection and the electron overflow issues can be improved due to the reversed polarization-induced potential barrier for carrier transport in p-type electron blocking layer. Furthermore, the impacts of different grading directions and schemes on the device performance are investigated. Simulation results show that grading the Al composition linearly from 0.65 to 0.6 for the 12 nm-thick AlGaN quantum barriers along the (000-1) can well balance the quantum barrier height and slope, thus resulting in remarkable improvement of hole injection as well as 53.6% enhancement of optical output power. The proposed design provides a straightforward and effective solution to the electron overflow and hole injection issues, which shows promise in the pursuit of higher efficiency DUV LED.

Key words: Deep Ultraviolet Light-Emitting Diode(DUV LED); AlGaN; N-polar; Grading quantum barrier; Carrier manipulation

OCIS Codes: 230.3670; 250.5590; 160.6000

0 Introduction

UV light sources play an important role in modern life because of extensive applications like water disinfection, bio-medical detection, three-dimensional printer, and UV-curing[1-2]. Compared with the traditional UV sources based on mercury, AlGaN-based Deep Ultraviolet Light-Emitting Diodes (DUV LEDs) are compact, environment-friendly, and long-lasting[3-4]. However, DUV LEDs are still generally unsatisfactory for commercial applications due to the low External Quantum Efficiency (EQE) and output power. So far, the highest EQE can only reach 20.3% in the laboratory[5]. Amid major EQE constraints, one is the insufficient carrier concentration in the active region which relies on the carrier injection efficiency and carrier overflow level. For a typical III-nitride LED, the potential barriers in n/p-type layers and the Quantum Barriers (QBs) height in Multiple Quantum Wells (MQWs) crucially affect the electron/hole injection and overflow.

Specially, first, electrons tend to flow into the p-type layer from the active region and being wasted due to the high mobility[6-8]. As a result, a p-type Al-rich Electron Blocking Layer (EBL) is conventionally inserted to reduce the electron overflow except our recent work[9-11]. However, the AlGaN EBL also results in a large valence band barrier that will hinder hole injection[12-13]. To settle this issue, researchers have explored various band engineering schemes, including adopting decreased Al-grading EBL[14], inverted-V-shaped EBL[15], AlGaN/AlGaN superlattice EBL[16-17] and Graded Superlattice (GSL) EBL[18-19]. However, those approaches could inevitably suffer from complex epitaxial conditions or increase in device resistance. One alternative solution to the valence band barrier issue is to employ the N-polarity instead of the prevailing III-polarity as shown by studies of N-polar GaN/InGaN visible LEDs: due to the opposite spontaneous polarization, the p-type EBL exhibited higher conduction barrier and lower valence barrier simultaneouslyl[20-22]; besides, the opposite polarization in MQWs can generate lower injection barriers that facilitate the carrier injection, as well as higher potential barriers along the carrier flow direction to confine carriers[23-24]. To achieve high-quality N-polar materials and devices, various research groups have employed In-surfactants-assisted growth[25], varying V/III ratio on SiC[26], or misorientation angles of substrate[27]. Despite reportedly high oxygen levels as shallow donors[28-29], Yan et al. shows that adopting the N-polar p-AlGaN through polarization-induced hole doping in LEDs can lead to significantly enhanced hole concentration as well as electroluminescence intensity[30-31].

Second, for the active region, the QB bending resulting from the polarization-induced field can significantly impact the transport of carriers and device performance. One report found that a thicker QB can increase the conduction-band potential for the electrons while lower the valence-band potential for holes to improve the quantum efficiency[32]. Also, the last QB composed of the superlattice structure with thin wells and barriers can lead to enhanced hole injection efficiency and output power[33]. A symmetric composition-graded quantum barriers structure was also designed to increase the optical power due to the superior capability of electron confinement[34]. Recently, we have reported that the QBs of III-polar DUV LEDs can block or enhance the carrier injection into QWs with compositional grading[11].

While many studies have been carried for the III-polar DUV LEDs and N-polar visible LEDs, few have focused on the N-polar DUV LEDs. It is therefore important to study the EBL and active region of the N-polar DUV LEDs to explore opportunities for high device performance. In this study, composition grading schemes based on N-polar device are numerically investigated to achieve the carrier manipulation and performance enhancement. We begin with the comparison of the electron blocking and hole injection capability between III-polar and N-polar structures. With the finding that the N-polar structure possesses preferable carrier transport in EBL and carrier confinement in MQWs, we conduct detailed studies of the impact of different QB grading schemes on the carrier injection in MQWs with the N-polar structure. Eventually, we propose the N-polar DUV LED with grading QBs that manifests the high electron/hole concentration and exhibits better output performance.

1 Comparison of III-polar and N-polar DUV LEDs

To fundamentally investigate the carrier transport capability, the III-polar and N-polar devices are constructed and simulated separately. Their structures are the same except for the polarity, as shown in Fig.1. The diode structure on an AlN template begins with an n-type $Al_{0.6}Ga_{0.4}N$ (3 μm, [Si] = 5×10^{18} cm^{-3}) electron - injection layer , followed by MQW active region consisting of five pairs 3 - nm $Al_{0.5}Ga_{0.5}N$ QWs sandwiched by six pairs 12-nm $Al_{0.6}Ga_{0.4}N$ QBs. The p-type region comprises a p-$Al_{0.7}Ga_{0.3}N$ (20 nm, [Mg] = 3×10^{19} cm^{-3}) EBL layer, a p-$Al_{0.6}Ga_{0.4}N$ (100 nm, [Mg] = 2×10^{19} cm^{-3}) hole-injection layer, and a p-GaN (20 nm, [Mg] = 1×10^{20} cm^{-3}) contact layer. The designed III-polar and N-polar devices with a chip size of 300×300 μm^2 and the emission wavelength at 270 nm are set as Samples A and B, respectively.

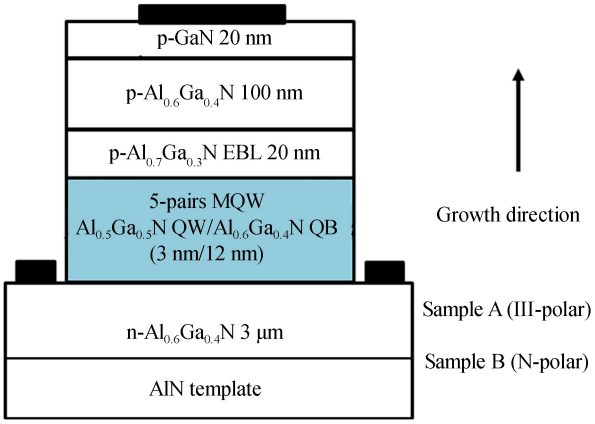

Fig.1 The cross-sectional schematics of Samples A and B based on the III-polar and N-polar DUV LED emitting at ~270 nm

For the device simulation, a commercial TCAD software, APSYS, developed by Crosslight Inc., was applied to build the simulation model[35]. In APSYS simulation, the calculated polarization-induced (including spontaneous and piezoelectric polarization) interface charges were based on the model contributed by Bernardini et al[36]. and Florentini et al[37]. For AlGaN materials, the bowing factor value and the band offset ratio were set to 0.94 and 0.58/0.42, respectively[38]. The electron and hole mobility values are determined based on the experimental data[39-40] and mobility model inside APSYS[41-42]. The activation energies of donors and acceptors in AlGaN were set according to the previous reports[39,43-44]. Effective mass value of electron and hole were provided by Punya et al[45]. Moreover, we set the radiative recombination coefficient, Auger recombination coefficient, Shockley-Read-Hall lifetime, and light extraction efficiency as 2.13×10^{-11} cm^3/s, 2.88×10^{-30} cm^6/s, 15 ns, and 10%, respectively[46]. 50% of the theoretical polarization charges due to the screening effect of defects were adopted for calculation[47]. Under the bias condition, the self-consistent quantum well models were taken into account.

Fig.2 depicts the energy-band diagrams of the two samples. It is clearly observed that the bending directions of Sample A (III-polar) and Sample B (N-polar) are opposite since the polarization-induced fields are reversed. In order to show the impact of EBL on the electron blocking and hole injection, we define the

electron-blocking-barrier (Φ_{Ee}) and hole-injection-barrier (Φ_{Eh}), which are corresponding with the energy difference between conduction/valence band of EBL and quasi-Fermi level in Fig. 2. For the electron-blocking-barrier (Φ_{Ee}), Sample B appears to have relatively higher value (370 meV) compared with that of Sample A (264 meV), which means Sample B has stronger electron blocking ability to suppress the electron overflow to the p-side. For valence band in EBL, holes in Sample A have a higher hole-injection-barrier (Φ_{Eh}=355 meV) to reach the active region from p-type layer while the case in Sample B is lower (Φ_{Eh}=332 meV), that will help the holes to be injected into MQWs.

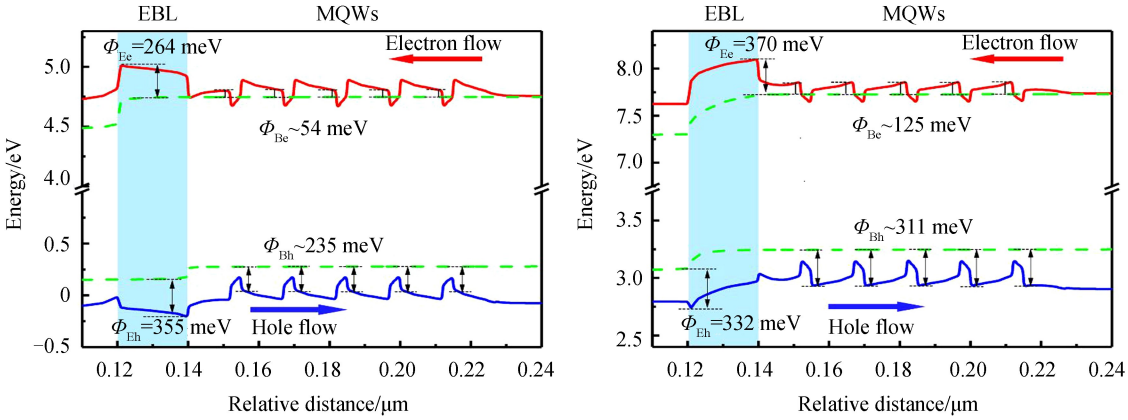

Fig.2 Energy-band diagrams of EBL and MQWs parts in Sample A and B at 180 mA

After injection into the QWs, the electrons and holes are accumulated towards different directions determinated by the polarization field both in the III-polar/N-polar QWs, i.e. the Quantum-Confined Stark Effect (QCSE). In the III-polar device, injected electrons are accumulated near the p-side and holes are accumulated near the n-side, that are also corresponding to the directions of electron and hole flow. To confine the carriers in QWs, conduction/valence band offsets relative to quasi-Fermi level form the electron-flow-barriers(Φ_{Be}) and hole-flow-barriers(Φ_{Bh}) along the direction of carrier flow, which are averagely 54 meV for electron and 235 meV for hole in Fig.2 (a). Nevertheless, in the N-polar case, the carrier flow barriers come from both the band offsets and polarization-induced bending in QWs, which show 125 meV for electron (Φ_{Be}) and 311 meV for hole (Φ_{Bh}). Moreover, the injected electrons and holes in Fig.2(b) are confined near the n-side and p-side, respectively, being kept away from the carrier flow barriers. It is clear that, in the N-polar case, the higher carrier flow barriers and being away from the barriers for carriers in QWs can reduce the likelihood of overflowing and significantly help the enhancement of quantum confinement [23].

Fig.3(a) and (b) show the carrier concentration [N_{QW}] and [P_{QW}] in the QWs. It can be found that the relative positions of the [N_{QW}] and [P_{QW}] peak are consistent with the different bending direction of band diagram. For comparison of electron and hole concentration, [N_{QW}] in QWs is totally larger than [P_{QW}] due to the active energy of Mg for p-doping is much higher than Si for n-doping in AlGaN[48]. Specifically, Sample B exhibits higher [N_{QW}] and [P_{QW}] than Sample A. In terms of electrons, the higher Φ_{Ee} of EBL in Sample B can effectively hinder the electron leakage into p-type region. The higher electron-flow-barriers Φ_{Be} in MQWs also reinforce the electron confinement. Then, more localized electrons of Sample B in QWs show higher average [N_{QW}]. The effect of the aforementioned process also works for holes except that the lower Φ_{Eh} of EBL in Sample B benefits the hole injection into QWs. Despite that Sample B has higher Φ_{Ee} and Φ_{Be}, electrons which have large mobility can still overcome those barriers. Then, the [N_{QW}] of Sample B just increase slightly compared with that of Sample A in Fig.3(a). Fig.3(c) shows that Sample B has higher R_{rad} than Sample A, resulting from the enhanced carrier concentration, especially holes which dominate the radiative recombination.

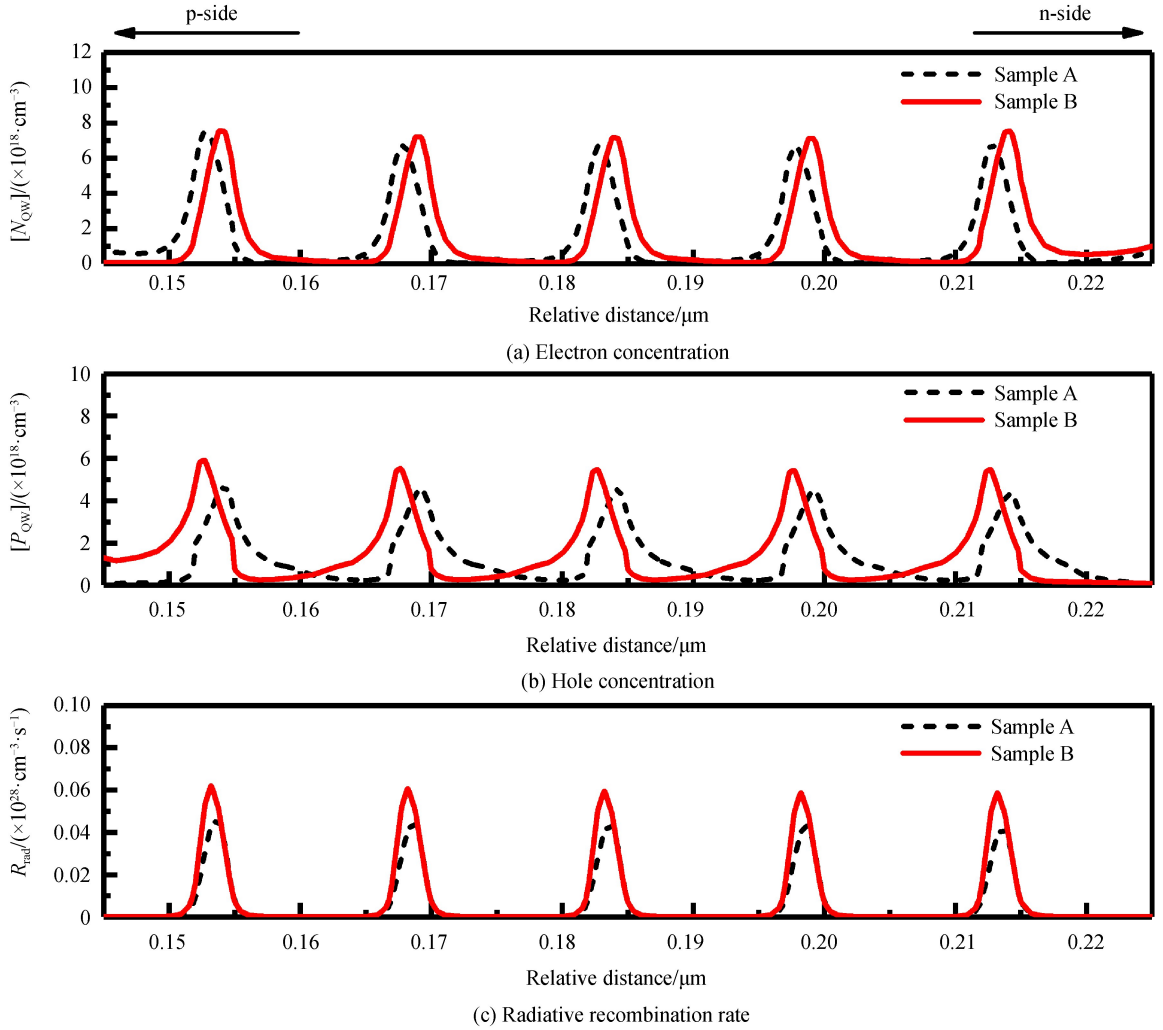

Fig.3 Carrier distribution and radiative recombination rate in MQWs of Samples A and B at 180 mA

The analyses of carrier concentration between Samples A and B demonstrate that the polarity of the device structure can considerably affect the EBL barriers (Φ_{Ee} and Φ_{Eh}) and MQWs barriers (Φ_{Be} and Φ_{Bh}), that in turn can significantly manipulate the carrier transport and recombination process. To obtain the straightforward evidence of suppressing electron overflow, the electron concentrations in the p-$Al_{0.6}Ga_{0.4}N$ layer, p-EBL, and last two QWs of the two samples are showed in Fig.4 (a). Notably, Sample B has much lower electron concentration from Last Quantum Barrier (LQB) to p-$Al_{0.6}Ga_{0.4}N$ layer than

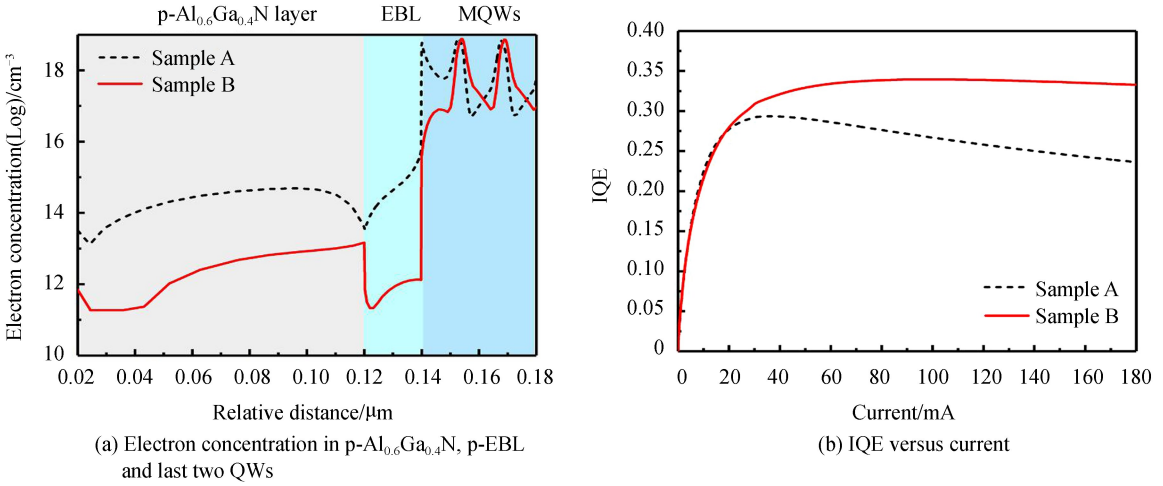

Fig.4 Electron concentration and IQE curve of Sample A and B

Sample A. The lower electron concentration clearly shows that the improved electron blocking ability of Sample B due to the applicable EBL barriers and higher MQWs barrier can well suppress the electrons into p-type region. It should also be noted that considerable electrons are accumulated on the interface of p-EBL and LQB in Sample A due to larger interface polarization charge and could become wasted. Fig.4 (b) shows the IQE curve of the two samples. Sample B has both higher IQE value and lower droop effect compared to Sample A, resulting from the enhanced R_{rad} in MQWs and the lower droop effect can be attributed to the improved electron overflow[8,49]. The proposed N-polar method can be applied in visible light emitting devices to show the advantages of improving carrier injection and output performance[24, 31]. However, this idea is more extensive in DUV region with Al-rich n-type and p-type AlGaN layers, which are suffering more from the doping difficulties.

2 N-polar DUV LED with composition-graded QB

Although the N-polar device can form desired barriers to confine more carriersin QWs, the steeper QBs can also block the carrier transport along the directions of carrier flow to some extent[11], especially for the holes which have much lower mobility than electrons. That means the barrier height for confining carriers and barrier slope for transporting carriers should be balanced. To further optimize the MQWs band diagram and improve the device performance, two types of QB grading schemes (increase or decrease Al-content) based on Sample B are constructed, as shown in Fig.5. The designed Samples have the same structures and settings in n-side and p-side but just differ in MQWs. One type of QB grading scheme has the linear composition grading from 0.6→x (x>0.6) along the growth direction while another one features on the linearly grading from y→0.6 (y>0.6) along the growth direction. It should be noted that all samples comprise five pairs 3-nm $Al_{0.5}Ga_{0.5}N$ QWs sandwiched by six pairs 12-nm AlGaN QBs. Specially, two Samples, denoted as Sample C (x=0.65) and Sample D (y=0.65) are built to detailedly analyze the carrier manipulation in MQWs in the following part.

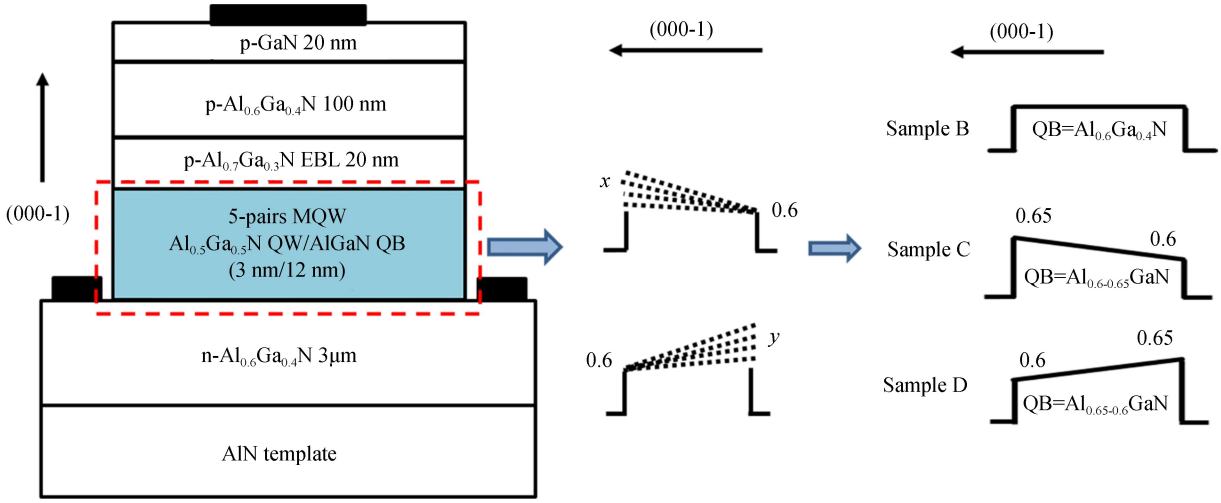

Fig.5 The cross-sectional schematic of N-polar DUV LED, Al-content profiles of designed samples with increase/decrease QB grading schemes

Fig.6(a) shows the output power of all structures designed in Fig.5. For the increasing composition grading scheme (0.6→x), the output performance keeps worse as x varies from 0.61 to 0.71. Nevertheless, when changing the beginning composition of y from 0.61 to 0.71, the output power shows an increasing tendency at first and then drops. The peak optical power happens at y=0.65 (Sample D's position). To investigate the influence of QBs grading on the carrier distribution and device performance, we take the band diagrams of Sample B, C, and D as a comparison, which are shown in Fig.6(b). Sample B is the reference structure without grading. Sample C (grading from 0.6→0.65) and Sample D (grading from 0.65→0.6) are specially designed structures. The three samples just differ in the MQWs part of the band diagram. The middle part in MQWs is zoomed in in Fig.6(c). The tilting degree of QBs can be assumed as the slope of QBs. For the conduction band, it can be observed that, with the compositional

grading along the growth direction, Sample C′s QBs become flatter, and the electron-flow-barriers (Φ_{Be}) are slightly higher than that of Sample B. Although Sample D′s Φ_{Be} show even higher value, the slope of Sample D′s QBs are also very large, which are determined by the dual effects of compositional grading and polarization-induced charge. For the valence band, both Sample C and Sample D show the opposite behavior of the conduction band. Sample C′s hole-flow-barriers (Φ_{Bh}) are the highest but the QBs slope are the steepest, while the Sample D′s Φ_{Bh} are moderate, but its QBs are the flattest. According to the previous analysis, if we just consider the impact of MQW barriers (Φ_{Be} and Φ_{Bh}), it can be easily predicted that Sample C and Sample D would have the largest hole and electron concentration in MQWs, respectively due to that the higher potential barriers can enhance the carrier confinement. However, the carrier distribution may not follow the predicted results because QBs slope (viewed as the tilting degree of QBs) also powerfully affects the carrier transport.

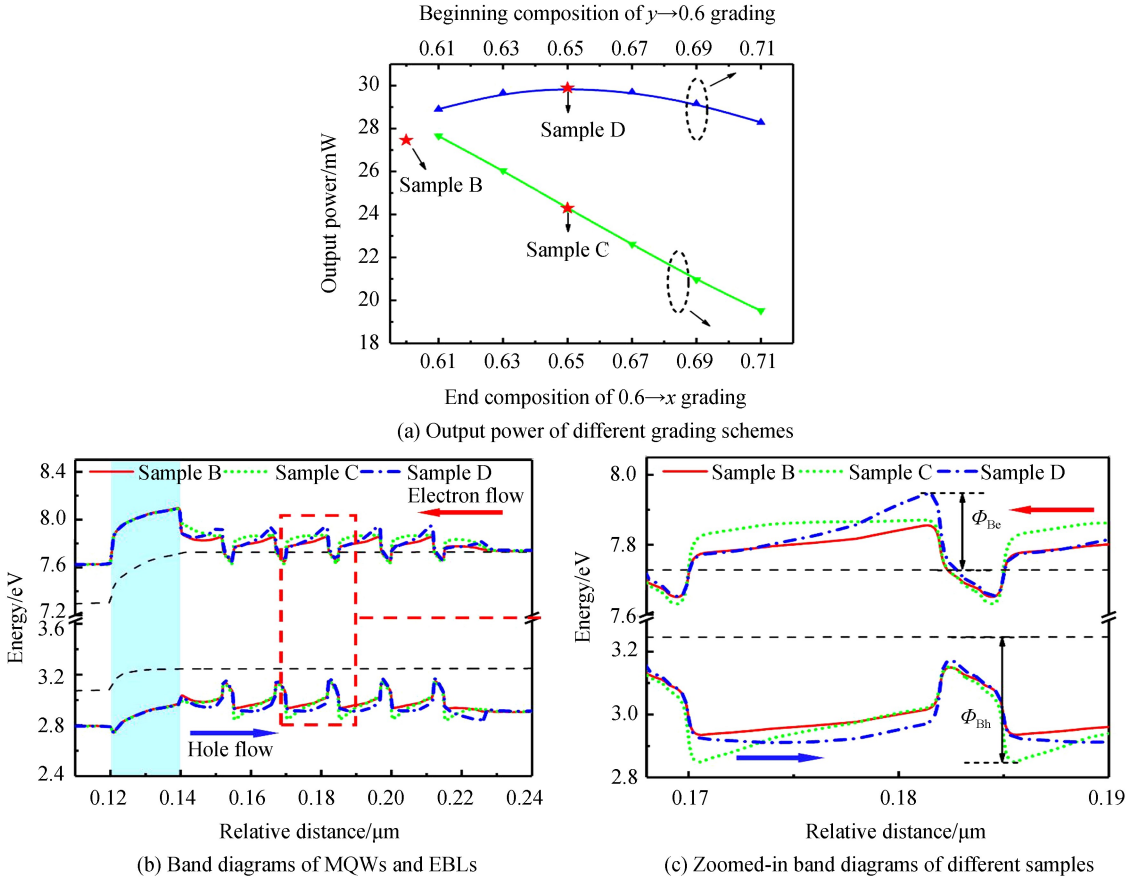

Fig.6 Output power of samples with different grading schemes, band diagrams of Sample B, C, and D

The simulated electron concentration [N_{QW}] and the hole concentration [P_{QW}] in the active region of Samples B, C and D are shown in Fig.7(a)～(b). Interestingly, Among the three samples, Sample C possesses the highest electron concentration while Sample D shows the highest hole concentration, which are totally inverse of the prediction above. Sample B always appears the intermediate behavior. In particular, for electrons, although Sample D has the highest electron-flow-barriers (Φ_{Be}) for confining the electrons, the steeper QBs of Sample D can inevitably block the electron transport in MQWs, resulting in slightly lower [N_{QW}] of Sample D in comparison to Sample B. As for Sample C, owing to the moderate Φ_{Be} and flatter QB that can facilitate the electron confinement and electron injection in QWs, Sample C′s [N_{QW}] is much higher. For holes, they are basically a similar situation with electrons. Sample D possesses the highest [P_{QW}] due to the preferable balance between flatter QBs and moderate Φ_{Be}. As for Sample C, the slightly lower [P_{QW}] than that of Sample B is attributed to the reason that the higher potential barriers (Φ_{Bh}) are compensated by the steeper QBs. Eventually, Sample D shows the highest R_{rad} due to the much higher [P_{QW}] than that of Sample B and C, as shown in Fig.7(c). Therefore, as the end composition x increases in Fig.6(a), the higher and higher QB valence slopes will block the hole injection, thereby

keeping deteriorating the device performance. In another case when y increasing from 0.61 to 0.65, the improved hole injection facilitates the output power, but when y exceeds 0.65, the electron may turn to the minority carrier in the radiative recombination process due to the impact of steeper conduction of QBs.

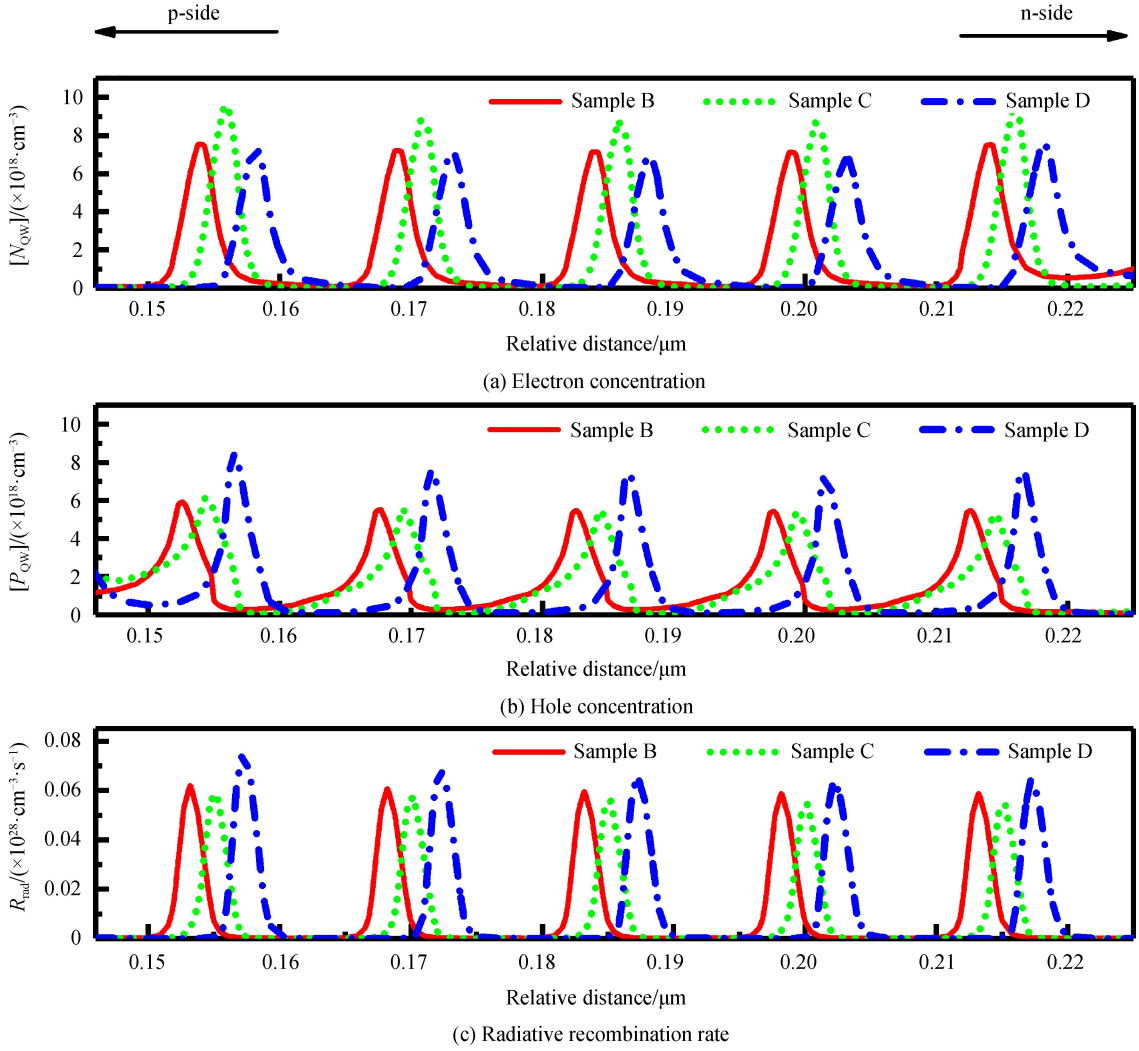

Fig.7 Carrier distribution and radiative recombination rate in MQWs of Samples B, C and D at 180 mA. The relative positions of Sample C and D are shifted 2 nm and 4 nm, respectively towards n-side for clear comparison

Fig.8(a) depicts the spontaneous emission rate of Samples A, B, C, and D. Those spontaneous emission rate spectra are integrated over all emission wavelengths from the quantum well. The peak emission wavelengths of the four samples are located at around 270 nm. But the peak wavelength of Sample B, C, and D with N-polar device shifts a little due to its reversed polarization-induced field that affecting the interband transition energy. Obviously, Sample D exhibits the highest spontaneous emission rate with respect to the other three samples due to the improved radiative recombination rate R_{rad}. For the output power versus injection current in Fig.8(b), Sample D shows the highest optical power among all samples, which coincides with the spontaneous emission rate in Fig.8(a). Eventually, due to the improved electron blocking and hole injection abilities, 53.6% higher output power is achieved for the designed N-polar DUV LED with decreased compositional grading structure (Sample D) than that of the conventional structure (Sample A), showing the promise of the N-polar structure with composition-graded QBs.

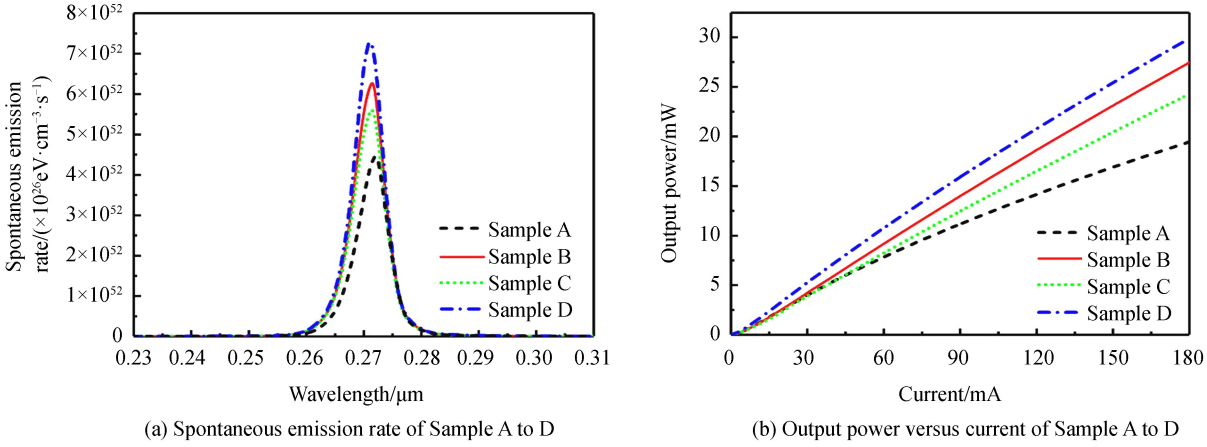

(a) Spontaneous emission rate of Sample A to D

(b) Output power versus current of Sample A to D

Fig.8 Spontaneous emission rate and output power of Sample A, B, C, and D

The compositional grading QBs in the N-polar structure reflects different characteristic and tendency when varying grading schemes in comparison to that of III-polar case[11], as well as showing emphasis of the balance between carrier flow barriers and QBs slope. It should be noted that, despite that the electron-containing-ability of grading QBs may contribute to the EBL-free devices[11, 19], the N-polar EBL shows huge superiority on the carrier manipulation, and it is one of the key points in this work.

Although the proposed solutions have been theoretically proved to be straightforward, it should be noted that some potential problems and obstacles of N-polar structure may exsit and are waiting to be overcome during the process of experimental implementation. First, the surface roughness and dislocation density of N-polar III-nitride film should be improved, which has been shown through misoriented substrate[50-51], substrate nitridation[52-53], and epitaxial lateral overgrowth (ELOG)[54]. Mowever, it is essential to control the nitrogen polarity with reduced inversion domains during the initial growth[55-56]. In addition, the optimizations of novel metal system and annealing condition are required for ohmic contact in N-polar film compared with mature Ga-polar case[57-59]. To promote the hole concentration in N-polar film, the studies of controlling oxygen incorporation[60] and polarization-doping[31] show the promise. This work may stop at the structure design, however, in practice people can take advantage of this carrier manipulation property based on the optimized growth technologies for higher performance LED.

3 Conclusions

To address the issues related to the carrier concentration including poor carrier injection, overflown carriers, and carrier confinement, we propose the N-polar grading AlGaN QBs DUV LED aiming at the polarization engineering in p-type EBL and MQWs. By employing the N-polar structure, the injected hole concentration in the active region can be significantly improved and electron leakage into p-type layer can be suppressed due to the reversed polarization-induced potential barrier for carrier transport in p-type EBL. Meanwhile, the quantum confinement of accumulated carriers in MQWs is also strengthened, stemming from the formed higher potential barriers along the carrier flow direction. In addition, with decreased Al-content grading along the growth direction in QBs, the injected hole concentration is further enhanced due to the preferable balance between flatter QBs and potential barriers in valence band, that can lead to the 53.6% higher output power as opposed to the conventional DUV LED. Through the systematic study, we have revealed the mechanism and impact of the N-polar structure and QB grading on the carrier manipulation. The proposed design in this work is effective and promising, that can direct the DUV research community to solve the inefficient carrier concentration issue and realize highly efficient DUV LEDs.

Reference

[1] MOUSTAKAS T D, PAIELLA R. Optoelectronic device physics and technology of nitride semiconductors from the UV to the terahertz[J]. *Reports on Progress in Physics*, 2017, **80**(10): 106501.

[2] PARK J-S, KIM J K, CHO J, *et al*. Review-group III-nitride-based ultraviolet light-emitting diodes: ways of increasing external quantum efficiency[J]. *Ecs Journal of Solid State Science and Technology*, 2017, **6**(4): Q42-Q52.

[3] KHAN A, BALAKRISHNAN K, KATONA T. Ultraviolet light-emitting diodes based on group three nitrides[J]. *Nature Photonics*, 2008, **2**(2): 77-84.
[4] KNEISSL M, KOLBE T, CHUA C, *et al*. Advances in group III-nitride-based deep UV light-emitting diode technology [J]. *Semiconductor Science and Technology*, 2011, **26**(1): 014036.
[5] TAKANO T, MINO T, SAKAI J, *et al*. Deep-ultraviolet light-emitting diodes with external quantum efficiency higher than 20% at 275 nm achieved by improving light-extraction efficiency[J]. *Applied Physics Express*, 2017, **10**(3): 031002.
[6] SZE S M, NG K K. Physics of semiconductor devices[M]. John Wiley & Sons, 2006.
[7] SHERVIN S, OH S K, PARK H J, *et al*. Flexible deep-ultraviolet light-emitting diodes for significant improvement of quantum efficiencies by external bending[J]. *Journal of Physics D: Applied Physics*, 2018, **51**(10): 105105.
[8] KIM M H, SCHUBERT M F, DAI Q, *et al*. Origin of efficiency droop in GaN-based light-emitting diodes[J]. *Applied Physics Letters*, 2007, **91**(18): 183507.
[9] KUO Y K, CHANG J Y, TSAI M C. Enhancement in hole-injection efficiency of blue InGaN light-emitting diodes from reduced polarization by some specific designs for the electron blocking layer[J]. *Optics Letters*, 2010, **35**(19): 3285-3287.
[10] HIRAYAMA H, TSUKADA Y, MAEDA T, *et al*. Marked enhancement in the efficiency of deep-ultraviolet AlGaN light-emitting diodes by using a multiquantum-barrier electron blocking layer[J]. *Applied Physics Express*, 2010, **3**(3): 031002.
[11] REN Z, LU Y, YAO H H, *et al*. III-nitride deep UV LED without electron blocking layer[J]. *IEEE Photonics Journal*, 2019, **11**(2): 8200511.
[12] LI L, ZHANG Y, XU S, *et al*. On the hole injection for III-nitride based deep ultraviolet light-emitting diodes[J]. *Materials*, 2017, **10**(10): 1221.
[13] ZHANG Z H, HUANG CHEN S W, ZHANG Y, *et al*. Hole transport manipulation to improve the hole injection for deep ultraviolet light-emitting diodes[J]. *Acs Photonics*, 2017, **4**(7): 1846-1850.
[14] ZHANG Y, YU L, LI K, *et al*. The improvement of deep-ultraviolet light-emitting diodes with gradually decreasing Al content in AlGaN electron blocking layers[J]. *Superlattices and Microstructures*, 2015, **82**: 151-157.
[15] FAN X, SUN H, LI X, *et al*. Efficiency improvements in AlGaN-based deep ultraviolet light-emitting diodes using inverted-V-shaped graded Al composition electron blocking layer[J]. *Superlattices and Microstructures*, 2015, **88**: 467-473.
[16] YIN Y A, WANG N, LI S, *et al*. Advantages of deep-UV AlGaN light-emitting diodes with an AlGaN/AlGaN superlattices electron blocking layer[J]. *Applied Physics A*, 2015, **119**(1): 41-44.
[17] ZHANG Z H, CHEN S W H, CHU C, *et al*. Nearly efficiency-droop-free AlGaN-based ultraviolet light-emitting diodes with a specifically designed superlattice p-type electron blocking layer for high mg doping efficiency [J]. *Nanoscale Research Letters*, 2018, **13**(1): 122.
[18] JANJUA B, NG T K, ALYAMANI A Y, *et al*. Enhancing carrier injection using graded superlattice electron blocking layer for UVB light-emitting diodes[J]. *IEEE Photonics Journal*, 2014, **6**(6): 1-12.
[19] ZHANG X, SUN H, HUANG J, *et al*. Efficiency improvements in AlGaN-based deep-ultraviolet light-emitting diodes with graded superlattice last quantum barrier and without electron blocking layer[J]. *Journal of Electronic Materials*, 2019, **48**(7): 460-466.
[20] MASUI H, KELLER S, FELLOWS N, *et al*. Luminescence characteristics of N-Polar GaN and InGaN films grown by metal organic chemical vapor deposition[J]. *Japanese Journal of Applied Physics*, 2009, **48**(7R): 071003.
[21] AKYOL F, NATH D N, GÜR E, *et al*. N-polar III-nitride green (540 nm) light emitting diode[J]. *Japanese Journal of Applied Physics*, 2011, **50**(5R): 052101.
[22] FENG S W, LIAO P H, LEUNG B, *et al*. Efficient carrier relaxation and fast carrier recombination of N-polar InGaN/GaN light emitting diodes[J]. *Journal of Applied Physics*, 2015, **118**(4): 043104.
[23] AKYOL F, NATH D, KRISHNAMOORTHY S, *et al*. Suppression of electron overflow and efficiency droop in N-polar GaN green light emitting diodes[J]. *Applied Physics Letters*, 2012, **100**(11): 111118.
[24] VERMA J, SIMON J, PROTASENKO V, *et al*. N-polar III-nitride quantum well light-emitting diodes with polarization-induced doping[J]. *Applied Physics Letters*, 2011, **99**(17): 171104.
[25] WON D, WENG X, REDWING J M. Metalorganic chemical vapor deposition of N-polar GaN films on vicinal SiC substrates using indium surfactants[J]. *Applied Physics Letters*, 2012, **100**(2): 021913.
[26] DENG G, ZHANG Y, YU Y, *et al*. Significantly improved surface morphology of N-polar GaN film grown on SiC substrate by the optimization of V/III ratio[J]. *Applied Physics Letters*, 2018, **112**(15): 151607.
[27] KELLER S, FICHTENBAUM N, WU F, *et al*. Influence of the substrate misorientation on the properties of N-polar GaN films grown by metal organic chemical vapor deposition[J]. *Journal of Applied Physics*, 2007, **102**(8): 083546.
[28] ZYWIETZ T K, NEUGEBAUER J, SCHEFFLER M. The adsorption of oxygen at GaN surfaces[J]. *Applied Physics*

Letters, 1999, **74**(12): 1695-1697.

[29] FICHTENBAUM N, MATES T, KELLER S, *et al*. Impurity incorporation in heteroepitaxial N-face and Ga-face GaN films grown by metalorganic chemical vapor deposition[J]. *Journal of Crystal Growth*, 2008, **310**(6): 1124-1131.

[30] SIMON J, PROTASENKO V, LIAN C, *et al*. Polarization-induced hole doping in wide-band-gap uniaxial semiconductor heterostructures[J]. *Science*, 2010, **327**(5961): 60-64.

[31] YAN L, ZHANG Y, HAN X, *et al*. Polarization-induced hole doping in N-polar III-nitride LED grown by metalorganic chemical vapor deposition[J]. *Applied Physics Letters*, 2018, **112**(18): 182104.

[32] BAO X, SUN P, LIU S, *et al*. Performance improvements for AlGaN-based deep ultraviolet light-emitting diodes with the p-type and thickened last quantum barrier[J]. *IEEE Photonics Journal*, 2015, **7**(1): 1-10.

[33] CHEN S, LI Y, TIAN W, *et al*. Numerical analysis on the effects of multi-quantum last barriers in AlGaN-based ultraviolet light-emitting diodes[J]. *Applied Physics A*, 2015, **118**(4): 1357-1363.

[34] CHANG J Y, CHANG H T, SHIH Y H, *et al*. Efficient carrier confinement in deep-ultraviolet light-emitting diodes with composition-graded configuration[J]. *IEEE Transactions on Electron Devices*, 2017, **64**(12): 4980-4984.

[35] MANUAL A U S. Crosslight software inc[M]. Burnaby, BC, Canada, 2013.

[36] BERNARDINI F, FIORENTINI V, VANDERBILT D. Spontaneous polarization and piezoelectric constants of III-V nitrides[J]. *Physical Review B*, 1997, **56**(16): R10024.

[37] FIORENTINI V, BERNARDINI F, AMBACHER O. Evidence for nonlinear macroscopic polarization in III – V nitride alloy heterostructures[J]. *Applied Physics Letters*, 2002, **80**(7): 1204-1206.

[38] COUGHLAN C, SCHULZ S, CARO M A, *et al*. Band gap bowing and optical polarization switching in Al Ga N alloys [J]. *Physica Status Solidi B*, 2015, **252**(5): 879-884.

[39] COLLAZO R, MITA S, XIE J, *et al*. Progress on n-type doping of AlGaN alloys on AlN single crystal substrates for UV optoelectronic applications[J]. *Physica Status Solidi C*, 2011, **8**(7-8): 2031-2033.

[40] NAKARMI M, KIM K, KHIZAR M, *et al*. Electrical and optical properties of Mg-doped Al 0.7 Ga 0.3 N alloys[J]. *Applied Physics Letters*, 2005, **86**(9): 092108.

[41] TURIN V O. A modified transferred-electron high-field mobility model for GaN devices simulation[J]. *Solid-State Electronics*, 2005, **49**(10): 1678-1682.

[42] CANALI C, MAJNI G, MINDER R, *et al*. Electron and hole drift velocity measurements in silicon and their empirical relation to electric field and temperature[J]. *IEEE Transactions on Electron Devices*, 1975, **22**(11): 1045-1047.

[43] KINOSHITA T, OBATA T, YANAGI H, *et al*. High p-type conduction in high-Al content Mg-doped AlGaN[J]. *Applied Physics Letters*, 2013, **102**(1): 012105.

[44] KOZODOY P, XING H, DENBAARS S P, *et al*. Heavy doping effects in Mg-doped GaN[J]. *Journal of Applied Physics*, 2000, **87**(4): 1832-1835.

[45] PUNYA A, LAMBRECHT W R. Valence band effective-mass Hamiltonians for the group-III nitrides from quasiparticle self-consistent G W band structures[J]. *Physical Review B*, 2012, **85**(19): 195147.

[46] YUN J, SHIM J I, HIRAYAMA H. Analysis of efficiency droop in 280-nm AlGaN multiple-quantum-well light-emitting diodes based on carrier rate equation[J]. *Applied Physics Express*, 2015, **8**(2): 022104.

[47] PIPREK J, FARRELL R, DENBAARS S, *et al*. Effects of built-in polarization on InGaN-GaN vertical-cavity surface-emitting lasers[J]. *IEEE Photonics Technology Letters*, 2006, **18**(1): 7-9.

[48] NAKARMI M, NEPAL N, LIN J, *et al*. Photoluminescence studies of impurity transitions in Mg-doped AlGaN alloys [J]. *Applied Physics Letters*, 2009, **94**(9): 091903.

[49] VERZELLESI G, SAGUATTI D, MENEGHINI M, *et al*. Efficiency droop in InGaN/GaN blue light-emitting diodes: Physical mechanisms and remedies[J]. *Journal of Applied Physics*, 2013, **114**(7): 10.

[50] ZAUNER A, WEYHER J, PLOMP M, *et al*. Homo-epitaxial GaN growth on exact and misoriented single crystals: suppression of hillock formation[J]. *Journal of Crystal Growth*, 2000, **210**(4): 435-443.

[51] ZAUNER A, ARET E, VAN ENCKEVORT W, *et al*. Homo-epitaxial growth on the N-face of GaN single crystals: the influence of the misorientation on the surface morphology[J]. *Journal of Crystal Growth*, 2002, **240**(1-2): 14-21.

[52] TAKEUCHI M, SHIMIZU H, KAJITANI R, *et al*. Al-and N-polar AlN layers grown on c-plane sapphire substrates by modified flow-modulation MOCVD[J]. *Journal of Crystal Growth*, 2007, **305**(2): 360-365.

[53] WU Y, HANLON A, KAEDING J, *et al*. Effect of nitridation on polarity, microstructure, and morphology of AlN films[J]. *Applied Physics Letters*, 2004, **84**(6): 912-914.

[54] SONG J, YUAN G, XIONG K, *et al*. Epitaxial lateral overgrowth of nitrogen-polar (0001) GaN by metalorganic chemical vapor deposition[J]. *Crystal Growth & Design*, 2014, **14**(5): 2510-2515.

[55] STOLYARCHUK N, MARKURT T, COURVILLE A, *et al*. Impact of sapphire nitridation on formation of Al-polar inversion domains in N-polar AlN epitaxial layers[J]. *Journal of Applied Physics*, 2017, **122**(15): 155303.

[56] KUELLER V, KNAUER A, BRUNNER F, *et al*. Investigation of inversion domain formation in AlN grown on sapphire by MOVPE[J]. *Physica Status Solidi C*, 2012, **9**(3-4): 496-498.

[57] KIM H, RYOU J H, DUPUIS R D, *et al*. Electrical characteristics of contacts to thin film N-polar n-type GaN[J]. *Applied Physics Letters*, 2008, **93**(19): 192106.

[58] DASGUPTA S, NIDH I, BROWN D F, *et al*. Ultralow nonalloyed ohmic contact resistance to self aligned N-polar GaN high electron mobility transistors by In (Ga) N regrowth[J]. *Applied Physics Letters*, 2010, **96**(14): 143504.

[59] LIU J, FENG F, ZHOU Y, *et al*. Stability of Al/Ti/Au contacts to N-polar n-GaN of GaN based vertical light emitting diode on silicon substrate[J]. *Applied Physics Letters*, 2011, **99**(11): 111112.

[60] PTAK A, HOLBERT L, TING L, *et al*. Controlled oxygen doping of GaN using plasma assisted molecular-beam epitaxy[J]. *Applied Physics Letters*, 2001, **79**(17): 2740-2742.